# NO Emission during Oxy−Fuel Combustion of Lignite

**ARTICLE** *in* INDUSTRIAL & ENGINEERING CHEMISTRY RESEARCH · FEBRUARY 2008

Impact Factor: 2.59 · DOI: 10.1021/ie0711832



**4 AUTHORS**, INCLUDING:

Filip Johnsson
Chalmers University of Technology
**202** PUBLICATIONS **4,162** CITATIONS

SEE PROFILE

# NO Emission during Oxy-Fuel Combustion of Lignite

**Klas Andersson,* Fredrik Normann, Filip Johnsson, and Bo Leckner**

*Department of Energy and Environment, Division of Energy Technology, Chalmers University of Technology, SE-412 96 Göteborg, Sweden*

This work presents experimental results and modeling of the combustion chemistry of the oxy-fuel ($O_2/CO_2$ recycle) combustion process with a focus on the difference in NO formation between oxy-fired and air-fired conditions. Measurements were carried out in a 100 kW test unit, designed for oxy-fuel combustion with flue gas recycling. Gas concentration and temperature profiles in the furnace were measured during combustion of lignite. The tests comprise a reference test in air and three oxy-fuel cases with different oxygen fractions in the recycled feed gas. With the burner settings used, lignite oxy-combustion with a global oxygen fraction of 25 vol % in the feed gas results in flame temperatures close to those of air-firing. Similar to previous work, the NO emission [mg/MJ] during oxy-fuel operation is reduced to less than 30% of that of air-firing. Modeling shows that this reduction is caused by increased destruction of formed and recycled NO. The reverse Zeldovich mechanism was investigated by detailed modeling and was shown to significantly reduce NO at high temperature, given that the nitrogen content is low (low air leakage) and that the residence time is sufficient.



## Introduction

For a long time, the emission of $NO_x$ has been a major concern in association with thermal power production, and the mechanisms behind the formation and destruction of $NO_x$ have been subject to extensive investigations, as for example discussed by Glarborg et al.[1] and in references therein. More recently, the oxy-fuel combustion process has received attention as a promising technology for $CO_2$ capture from fossil fuel power plants (with subsequent storage of $CO_2$). To obtain high $CO_2$ concentration in the flue gas, nearly pure $O_2$ from cryogenic air separation is used instead of air to oxidize the fuel. Combustion temperatures similar to those of air-firing are achieved by mixing the $O_2$ with externally recycled flue gases (RFG), mainly consisting of $CO_2$. The RFG flow also contains moisture, $NO_x$, and $SO_x$, but the concentrations of these depend on fuel properties, flue gas treatment, and degree of accumulation in the recycle loop. If the concentrations of $NO_x$ and $SO_x$ are low enough to avoid secondary removal devices, cost savings can be made. It is therefore of interest to study the formation and destruction of such pollutants under different oxy-fuel conditions, using flue gas recycling and for different types of fuels. Yet, it should be mentioned that $NO_x$ and $SO_x$ removal during the $CO_2$ conditioning or simultaneous removal and storage with $CO_2$ could be even more cost-efficient, if successful. This option, although important, is not treated here.

Investigations of oxy-fuel combustion fundamentals have underlined some significant differences between air- and oxy-firing with regard to formation of emissions, as reviewed by Buhre et al.[2] (work up to 2004). $NO_x$ has been especially emphasized: it has been shown by experiments on both laboratory[3−12] and semitechnical scales[13−24] that a significant reduction can be achieved with oxy-fuel combustion compared to air-firing. Laboratory tests typically use bottled $O_2$ and $CO_2$ to simulate the oxy-fuel combustion environment in once-through systems without recycling. In such systems the typical accumulation of certain chemical compounds does not take place, and the conclusions presented[8,10] with respect to oxy-fuel combustion are that (i) the conversion of fuel-N to NO increases with increasing $O_2$ fraction in the feed gas and (ii) air staging, as a means to reduce $NO_x$, is equally effective in $O_2/CO_2$ as in air environments.

In some laboratory studies[3,5,6,9] NO was added to the $O_2/CO_2$ oxidants to simulate recycle of $NO_x$ in a boiler. Okazaki et al.[3] examined various effects on reduction of NO under recycling conditions and concluded that the influence of the high $CO_2$ concentration is negligible. Instead, an effect of the interaction of fuel-N and recycled NO was detected (it is said to account for 10−50% of the total reduction). Furthermore, it is concluded that reduction of NO to molecular $N_2$ due to chemical reactions in the combustion zone is the main reason for the overall decrease (50−80%) in NO during recycling. Hu et al.[6] evaluated three coal types for a wide range of stoichiometries and found that the reduction efficiency of recycled NO ranges from 0.3 at a stoichiometric ratio ($\lambda$) of about 2 up to 0.8 at $\lambda \approx 0.7$, a feature that was rather independent of the coal tested. Several coal types have been tested,[9] for which the conversion of coal-N to NO varied from 50 to 90%. According to the authors, the conversion to NO seems to increase with the reactivity of the coal. Furthermore, it is concluded that the reduction of the recycled NO depends on the composition of the oxidant and on the combustion conditions, such as staging and location of the recycle inlet.

Work on a semitechnical scale, applying flue gas recycling, generally achieves a reduction of the $NO_x$ emission between 50 and 80% for oxy-fuel combustion compared to air-firing. An early study[18] discusses the differences in $NO_x$ production for air and oxy-fuel environments based on measurements of HCN and $NH_3$ in a flame. They conclude that, in the flame zone, $NO_x$ is rapidly reduced to HCN or $NH_3$ and that this is the reason for the reduction of the recycled $NO_x$. In a study by Kiga et al.[19] $\lambda$ was varied from 0.8 to 1.2 with a rather small effect on the overall conversion of fuel-N to $NO_x$ in contrast to air-firing, where the conversion was more than 3-fold at $\lambda = 1.2$ compared to $\lambda = 0.85$. To date, few studies have combined experiments and modeling of the nitrogen chemistry during oxy-coal combustion. However, Chui et al.[21] compares experiments in a 300 kW test unit with CFD modeling results including $NO_x$

* To whom correspondence should be addressed. E-mail: Klas.Andersson@me.chalmers.se.

10.1021/ie0711832 CCC: $40.75 
Published on Web 02/16/2008

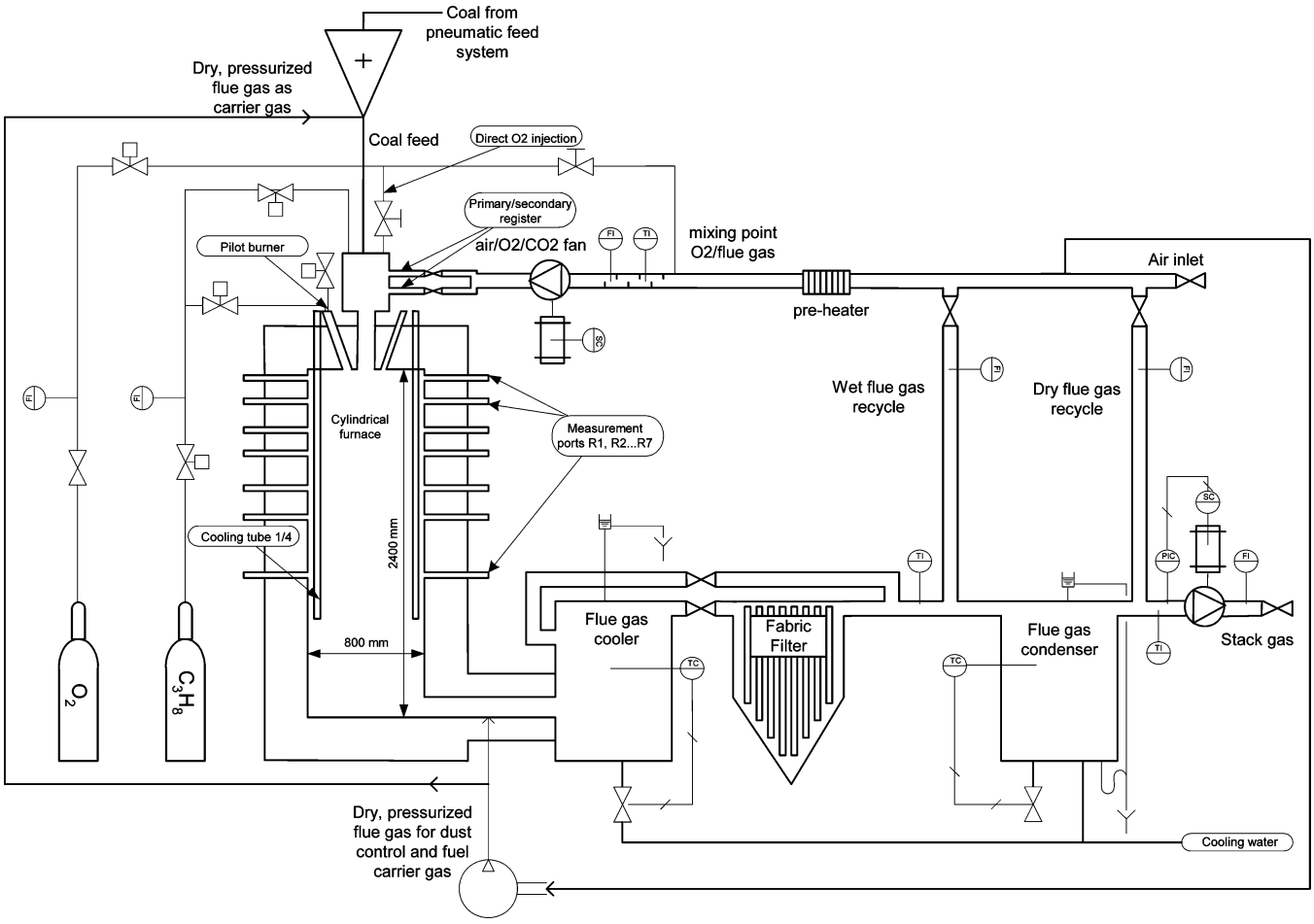


**Figure 1.** Chalmers 100 kW oxy-fuel combustion test unit.

**Table 1. Fuel Properties**

| fuel analysis | | | | | | | | | |
|---|---|---|---|---|---|---|---|---|---|
| | proximate [wt %, as received] | | | | ultimate [wt %, daf] | | | | |
| $H_i$ [MJ/kg] (as received) | moisture | ash | combustibles | % daf volatile matter | C | H | N | S | O |
| 20.9 | 10.2 | 5.0 | 84.8 | 59.4 | 69.9 | 5.4 | 0.6 | 1.0 | 23.1 |

predictions. The authors claim an acceptable agreement between experiments and modeling. A similar study by Chui et al.[22] compares modeled and experimentally derived NO data in an evaluation of different burner concepts for oxy-fuel firing. It is clear that the burner design has a significant impact on the $NO_x$ emission under both air-fuel and oxy-fuel conditions.

The present work discusses the active mechanisms in the formation and destruction of NO during oxy-fuel combustion. A simple model is established to evaluate measurement data from a 100 kW combustor. Furthermore, the gas phase reactions, participating in the nitrogen chemistry, are simulated by a detailed chemical kinetic scheme under conditions that are not included in the experiments. The purpose is to study the sensitivity of NO formation to temperature, residence time, stoichiometry, recycle rate, and air leakage. These parameters are relevant for optimization of the oxy-fuel combustion process, and their influence on the overall formation of NO is therefore of importance. The work also aims at mapping gas phase destruction routes of NO during oxy-fuel combustion in order to identify suitable process conditions for further NO reduction by primary measures.

## Experiments

The 100 kW test facility (Figure 1) can be run with both gaseous and pulverized fuels. Since previous work on propane,[25] a new fuel-feed system, a dust-blowing system, and a fly ash fabric filter have been installed for operation with pulverized fuels. A small conical bluff body has been added to the burner tip to stabilize the flame during firing of lignite. The main geometries of the combustor (inner diameter 0.8 m, inner height 2.4 m) and the swirl settings of the burner are the same as in previous work with gas (see Andersson and Johnsson[25] for further details). The gas for coal transport is composed of dried recycled flue gas, which is mixed with fresh $O_2$ before the gas/coal mixture enters the combustion chamber. The $O_2$ fraction in the carrier gas was 30 vol % in all oxy-fuel test cases. The experiments presented here were performed under dry recycling conditions. The oxidizer was supplied without preheating. The fuel was predried German lignite (see Table 1), and the oxygen purity was 99.5 vol %. The test conditions are summarized in Table 2. The reference condition is air combustion, which is compared to three oxy-fuel cases, termed OF 25, OF 27, and OF 29, where the numbers express the oxygen concentration in volumetric percent. The oxygen fraction in each case was

**Table 2. Measurement Conditions in the Test Series**

| | | | target feed gas composition [vol %] | | | |
|---|---|---|---|---|---|---|
| test case | combustion media | stoichiometric ratio, $\lambda$ | $O_2$ | $N_2$ | $CO_2$ | target $O_2$ excess in flue gas [vol %] |
| air | air | 1.18 | 21 | 79 | | 3.1 |
| OF 25 | $O_2/CO_2$ dry recycle | 1.18 | 25 | | 73 | 3.7 |
| OF 27 | $O_2/CO_2$ dry recycle | 1.18/1.30/1.41 | 27 | | 71 | 3.9/6.0/8.0 |
| OF 29 | $O_2/CO_2$ dry recycle | 1.18 | 29 | | 69 | 4.2 |

**Table 3. Measurement Positions on the Combustor**

| port | dist from burner [mm] |
|---|---|
| R1 | 46 |
| R2 | 215 |
| R3 | 384 |
| R4 | 553 |
| R5 | 800 |
| R6 | 998 |
| R7 | 1400 |

obtained by varying the flue gas recycle rate while maintaining a constant stoichiometry. Additional tests were made in the OF 27 case with different stoichiometries both with and without air leakage. The effect of air leakage was tested by replacing the $O_2/CO_2$ carrier gas mixture with air, corresponding to a leakage flow of approximately 4 vol % of the total inlet flow. The three oxygen fractions in the RFG (or the recycle rates) were chosen on the condition (1) that similar furnace temperatures were achieved for OF 25 and air-firing, (2) of avoiding flame stability problems that started to occur when the recycle rate was increased from the OF 25 case toward lower oxygen concentrations in the RFG (the stoichiometry was kept constant), and (3) of avoiding the ash melting temperature (~1350 °C) that was approached when the recycle rate was decreased from OF 25 to reach OF 29 conditions. The third condition was employed since ash melting is a practical problem during in-flame measurements with cooled probes, such as the ones used in the present work.

Table 3 shows the axial distance from the burner inlet to the ports for radial temperature and gas composition measurement. The temperature was measured with a suction pyrometer (Figure 2) equipped with a type S thermocouple, shielded with three concentric ceramic tubes to prevent radiative heat loss from the thermocouple junction. The on-line gas analyzers for $O_2$, CO, $CO_2$, NO, and total hydrocarbon (THC) concentrations are specified in Table 4. Due to the wide range of $O_2$, CO, and $CO_2$ concentrations, two analyzers were used for these components.

The gas sampling probe (Figure 3) consists of a heated inner tube with controlled temperature to prevent condensation inside the probe and an outer protecting water-cooled jacket with a diameter of 45 mm. The gas is sucked through a 4 mm thick ceramic filter on the tip of the probe, after which it is dried, filtered, and fed into the gas analyzers. The $O_2$ excess in the stack gas is monitored throughout the measurements. It typically varies by ±0.1 vol % during air-firing and by ±0.3 vol % during oxy-firing, which illustrates the well-controlled conditions prevailing. Fluctuations in the flue gas composition, typical during air-firing, are magnified in oxy-combustion owing to the nature of the semiclosed oxy-fuel process; the variations in the flows entering the system must be reduced as much as possible to maintain the desired stoichiometry (here, $\lambda = 1.18$), and the $O_2$ fraction in the feed gas within narrow limits of variation. The importance of the control of the feed systems, especially the coal flow, should not be underestimated during oxy-fuel operation.

The NO emission is given in both parts per million [ppm] and milligrams per megajoules [mg/MJ]. During oxy-fuel operation the NO emission in mg/MJ, $E_{NO}$, is calculated as

$$E_{NO} = \frac{M_{FG} X_{NO}}{H_i} \tag{1}$$

where $M_{FG}$ is the dry flue gas yield produced per unit mass of

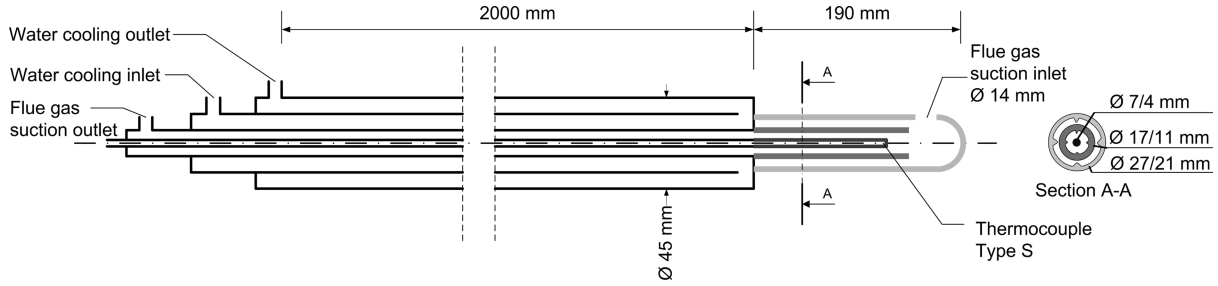


**Figure 2.** Suction pyrometer.

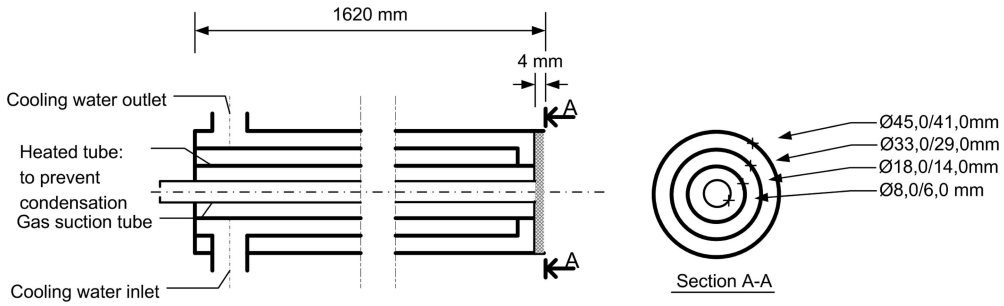


**Figure 3.** Gas sampling probe.

**Table 4. Gas Analysis Instruments, Measurement Ranges, and Specification of Calibration Gas**

| component | model | measurement principle | measurement range | span gas concn |
|---|---|---|---|---|
| $O_2$ | Fisher Rosemount (NGA 2000) | paramagnetic | 0−25% | 9.00% |
| $O_2$ | Binos (100 2M) | paramagnetic | 0−50% | 21.0% |
| $CO_2$ | Hartmann & Braun (Uras 10p) | NDIR | 0−20% | 18.0% |
| $CO_2$ | Binos (100 2M) | TC | 0−100% | 86.0% |
| CO | Hartmann & Braun (Uras 10P) | NDIR | 0−1.0% | 8998 ppm |
| CO | Hartmann & Braun (Uras 3K) | NDIR | 0−10% | 9.02% |
| CO | Sick Maihak (S 710) | NDIR | 0−1.0%, 0−2.0% | 8998 ppm |
| | | | 0−10%, 0−20% | 9.02% |
| THC | Rosemount Analytical (400 A) | FID | 0−10% | 4.94% |
| NO | ECO Physics (CLD 700 EL) | chemiluminescence | 0−1000 ppm | 400 ppm |

fuel, $X_{NO}$ is the measured fraction of NO in the flue gas (on dry basis), and $H_i$ is the lower heating value (given in Table 1).

## Modeling

The modeling is divided into a simplified NO model and a detailed NO chemistry model. The simplified NO model is a tool whose purpose is to evaluate the experimental results presented in this work and should describe the formation and reduction of NO in air and oxy-fuel combustion. The objective is to determine the importance of decreased formation versus increased destruction in the total NO reduction in oxy-fuel combustion. This model should be regarded as descriptive rather than predictive.

The detailed NO chemistry model aims at further investigating the gas phase reduction of NO during oxy-fuel combustion, under conditions that are not included in the experiments. The importance of reduction paths and of certain parameters is investigated by means of established kinetic data. The parameters are temperature, gas residence time in the reactor, stoichiometric ratio, and inlet concentration of nitric oxide and nitrogen to the reactor.

**1. $NO_x$ Formation.** NO is formed along three routes: thermal, prompt, and fuel-N. Thermal formation of NO from reactions between molecular $N_2$ and $O_2$ is described by the extended Zeldovich mechanism:

$$N_2 + O \leftrightarrow NO + N \quad (2)$$

$$N + O_2 \leftrightarrow NO + O \quad (3)$$

$$N + OH \leftrightarrow NO + H \quad (4)$$

Similar to thermal NO formation, the prompt route is closely related to the amount of free nitrogen available. Generally, it is only important under fuel-rich conditions. Fuel-bound nitrogen contributes significantly to the NO formed in air-fired combustion and even more during oxy-fuel combustion when the airborne $N_2$ is nearly or completely eliminated. Fuel-N reacts via volatile-N (Vol-N) and char-N to form NO. The distribution of NO formation from char and volatiles depends on combustion conditions and coal type. The important reaction steps of volatile-N involve one or more intermediary compounds, e.g., HCN, $NH_3$, or N, and subsequent reaction of these through competitive reaction paths to yield NO or $N_2$. Char-N reacts through a set of heterogeneous reactions to NO or $N_2$. Figure 4 shows the different reaction paths of fuel-N, where Vol-N is an intermediate gaseous compound. The split between $N_2$ and NO varies with type of coal and depends on qualities such as nitrogen content, coal rank, and volatility. The char is also important as a catalyst for destruction of NO, either directly or by reaction with CO or $H_2$.

Common primary measures to reduce $NO_x$ are the reburning (or fuel staging) and staged-combustion (or air-staging) methods. Reburning is normally executed by introducing a substoichiometric hydrocarbon flame downstream of the primary combustion zone in order to reduce NO according to the overall reaction

$$C_xH_yO_z + NO \rightarrow N_2 + ... \quad (5)$$

This procedure can be compared with the introduction of NO into the flame zone during oxy-fuel combustion with flue gas recycle. In staged combustion the oxidizer is staged rather than the fuel. This reduces the concentration of available oxygen in zones that are critical for NO formation, and also the amount of fuel burnt at the peak temperature. In addition, there are a number of secondary $NO_x$ reduction methods, such as selective catalytic reduction (SCR) and selective noncatalytic reduction (SNCR), which are not treated in this work.

**2. Evaluation of NO Data from Experiments.** In the evaluation of NO data, the combustion chamber is modeled in steady state and in one dimension. It is divided into six sections (Figure 5). The length of each section agrees with the length between the measurement ports (Table 3), allowing the use of measurement data as input to the calculations. A maximum temperature difference of 20% was used as the criterion to determine the lateral distribution of the modeled reactor section (MRS), represented by the white area in Figure 5, supported by the observed flame extension (see Figure 7a): the flame temperature is fairly constant in the high-temperature zone, but it decreases drastically at a distinct position in all flames in port 2. Even though differences can be observed in the $O_2$ and CO contents within the MRS, the mean value always captures the trend of the measured distribution. Outside the MRS, the temperature distribution and gas composition are strongly two-dimensional, but the temperature (see Figure 7a) and the fuel concentration are low, and the chemical reactions occurring in this region can be neglected.

With the purpose of focusing the model on NO chemistry, the reactions are treated in different ways. The lateral mean

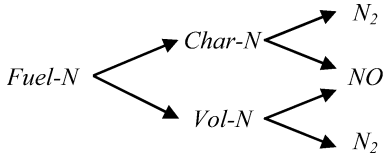


**Figure 4.** Overall mechanism for fuel-N.

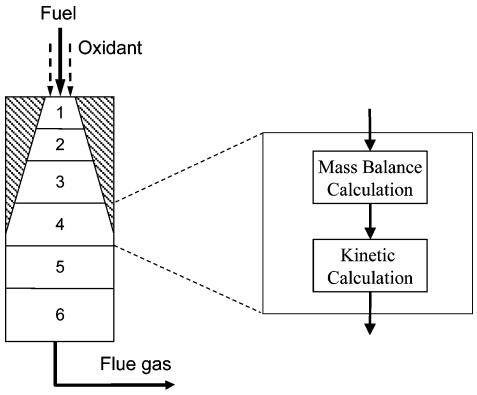


**Figure 5.** Combustion model and discretization of the reactor, including a scheme of the calculations performed in each section.

**Table 5. Investigated Properties in the Gas Phase Reaction Model**

| | |
|---|---|
| temperature | 800−2000 °C |
| stoichiometric ratio | 0.7−1.1 |
| residence time | 0−1 s |
| initial NO fraction | 200−1000 ppm |
| initial $N_2$ fraction | 0−15% |

concentrations of $O_2$ and CO from the measurements within the MRS are taken as input. The concentrations of substances with no direct importance to the NO chemistry involved, i.e., $H_2$, $H_2O$, and $CO_2$, are calculated with a mass balance between the measurement positions. This mass balance is followed by calculation of the formation and destruction of NO and $N_2$ expressed by reaction kinetics (for reactions 7−9). Each section is assumed to be a plug-flow reactor, whose initial values are taken from the previous calculation, and the residence time is obtained from the length and width of the given section. The temperature of the plug-flow reactor is assumed to increase linearly between the measurement positions.

The rate of reaction is expressed by

$$r = p_A p_B k_0 \exp\left(\frac{-E_A}{RT}\right) \quad (6)$$

where $p_A$ and $p_B$ are the partial pressures of the reactants, $k_0$ is the rate constant, and $E_A$ is the effective activation energy. The influence of the flow profile in the combustor is included in the reaction rate without the use of separate input parameters. This approach is acceptable as the model is not a predictive one, and the influence of the flow profile can be assumed to be constant throughout this study. The model is implemented in Aspen Plus,[26] applying the extensive database of physical properties and thermodynamic models included in this software.

The reduction of NO is modeled by

$$NO + XO \rightarrow (1/2)N_2 + O_2 \quad (7)$$

where XO represents several reactants in a reducing environment, including all mechanisms for NO reduction, e.g., the CO/char and the reburning mechanism. As a consequence of the experimental conditions, both the thermal and prompt formation routes make insignificant contributions to the NO formation. The reaction paths of the conversion of fuel-N are described by

$$2XN + O_2 \rightarrow 2NO \quad (8)$$

$$2XN \rightarrow N_2 \quad (9)$$

where XN represents all intermediate components evolving from fuel-N, including HCN, $NH_3$, and char-N. The fuel-bound

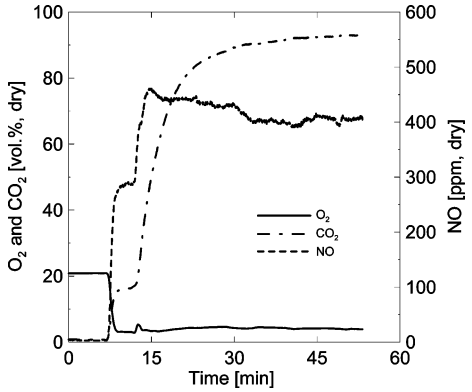


**Figure 6.** Gas composition in the flue gas during a start-up sequence from air-firing to oxy-fuel firing (OF 27 conditions).

**Table 6. Measured Gas Composition (Dry Basis) at the Inlet and Outlet of the Reactor**

| | measured dry gas composition at the reactor inlet/outlet (in/out) | | | | | | |
|---|---|---|---|---|---|---|---|
| | $O_2$ [vol %] | | $CO_2$ [vol %] | | measured temp | | |
| test case | in | out | in | out | in [°C] | out [°C] | peak [°C] |
| air | 21 | 3.1 | | 17 | 20 | 708 | 1222 |
| OF 25 | 25 | 3.7 | 72 | 94 | 23 | 625 | 1203 |
| OF 27 | 27 | 3.9 | 71 | 94 | 28 | 663 | 1261 |
| OF 29 | 29 | 4.2 | 69 | 94 | 20 | 645 | 1343 |

nitrogen is converted in two parallel irreversible reaction paths: one to NO and one to $N_2$. This is so, since only the selectivity between these paths is of interest. This simplistic model gives an understanding of the main features of the oxy-fuel process. Abbas et al.[27] have shown that simple models similar to the one above can give results that are in line with those of more advanced models.

**3. Detailed NO Chemistry Model.** In the detailed NO chemistry model, the system is modeled as a plug-flow reactor at constant temperature and pressure with the SENKIN[28] code of the CHEMKIN-II[29] software, an approach that has been validated against calculations by Glarborg et al.[30] A pure methane flame from an $O_2/CO_2$ mixture with an initial content of NO represents the gas phase environment. The gas phase reactions, involving nitrogen oxides, are investigated using a detailed chemical kinetic scheme[31] together with the associated thermodynamic library. The scheme involves 73 species in 520 elementary gas phase reactions and includes mechanisms for combustion of light hydrocarbons (C1 to C2) and the nitrogen mechanisms relevant for staged combustion, reburning, and SNCR. No heterogeneous gas−solid reactions (such as the char-CO reduction mechanism) are included. Methane is selected, being a simple hydrocarbon gas, as no decisive difference between methane and other hydrocarbon fuels has been established in the present context.[32] The values used for the calculation and the range of the parameters investigated are given in Table 5. The base case is calculated at a stoichiometric ratio of 0.9, atmospheric pressure, and a residence time of 0.5 s. The initial concentration of the oxidizer is set to 25% $O_2$ and 1000 ppm NO. The limits of the gas phase reduction of NO are also investigated by calculating the equilibrium gas phase concentration of NO in different $N_2$ atmospheres using the EQUIL[33] code and the fuel-N concentration in Table 1.

## Results

The results are presented in three parts: (1) experimental results from the 100 kW test unit, including overall NO emission data and distributions of radial temperature and gas composition in the furnace, used as input in the combustion modeling; (2) evaluation of experimental NO data, modeling of measurements to determine the overall formation, and reduction of NO under oxy-fuel conditions; and (3) detailed NO chemistry modeling, based on established mechanisms and providing a generalized knowledge on NO destruction routes for a wide range of oxy-fuel conditions.

**1. Experimental Results.** Table 6 shows the time-averaged measured dry gas compositions and temperatures at the inlet and outlet of the reactor in the main test cases (at $\lambda = 1.18$). The measured total gas concentration ($CO_2 + O_2$) varies between 97 and 98 vol %. Due to the presence of 0.5 vol % argon in the oxygen feed and the nitrogen introduced with the coal, the theoretical maximum of $CO_2 + O_2$ is just below 98.3 vol % on dry basis. The discrepancy of about 0.3−1.3 vol % between the actual gas concentration and the theoretical one

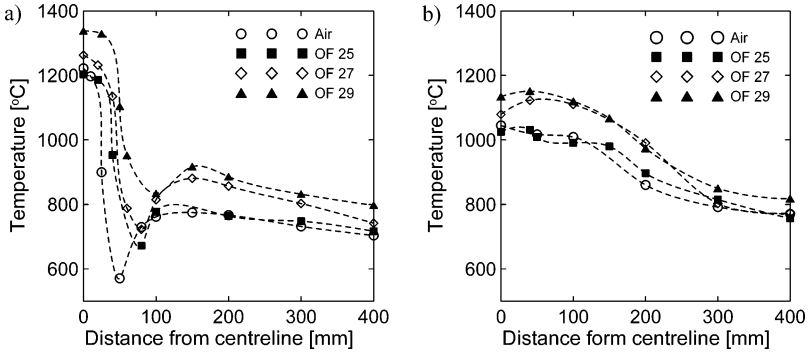


**Figure 7.** Radial temperature profiles measured at (a) 215 and (b) 553 mm from the burner inlet. The dashed lines are spline fits to the experimental data.

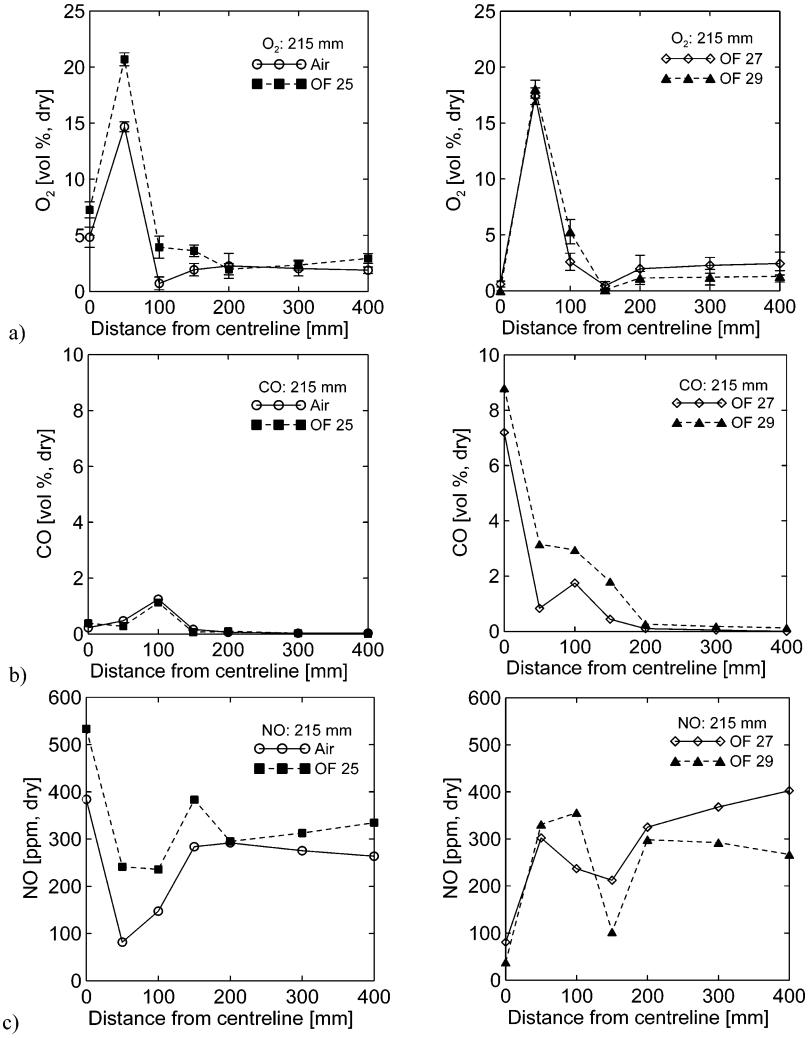


**Figure 8.** Measured radial gas concentration profiles 215 mm from the burner: (a) $O_2$, (b) CO, and (c) NO.



can be attributed to a small leakage of airborne $N_2$ into the system. It can be concluded that, in principle, this small leakage will not lead to formation of any thermal NO at the temperature level of the tests, a matter that will be further discussed in connection with the NO chemistry modeling.

Figure 6 shows the change of the $O_2$ excess in the flue gas together with the $CO_2$ and NO concentrations at the outlet of the reactor during a typical start-up sequence from air- to oxy-firing (OF 27). The two latter components are accumulated in the recirculation flow during recycle operation. First, the fans were adjusted to produce the desired flow conditions. After 8 min of operation the flame was ignited on air. The $CO_2$ and $O_2$ concentrations stabilized at about 17 and 3 vol %, and NO was just below 300 ppm (steady-state conditions were not quite reached due to the short operational time on air). The oxy-fuel operation started at about 13 min with $O_2$ injection into the combustion air, after which the RFG line was opened immediately. During a couple of minutes the $O_2$ feed increased as the air inlet valve was closed, causing a short peak in $O_2$ due to an overshoot in oxygen feed, which was kept temporarily to maintain a stable flame. The increased stoichiometric ratio during this period gave raise to a small peak also in the NO concentration. $CO_2$ reached a concentration above 90 vol % after about 20 min of operation, but final steady-state condition was typically achieved after a few hours of operation.

Figures 7 and 8 present cross-sectional temperatures and gas concentrations ($O_2$, CO, and NO) measured in ports 2 and 4 (215 and 553 mm from the burner inlet, respectively). Figure 7

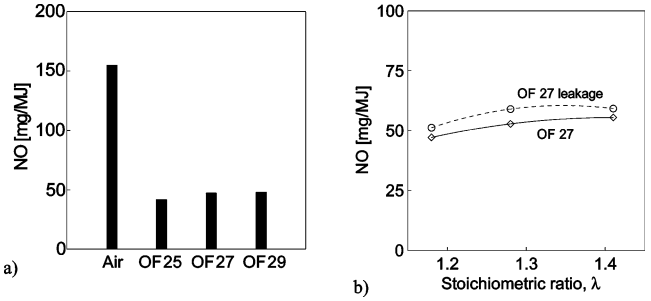


**Figure 9.** NO emission at the stack for (a) constant $\lambda = 1.18$ and (b) $\lambda$ varying between 1.18 and 1.41, with and without air leakage (≈4% of the feed gas flow).

shows that OF 25 is the oxy-fired condition with a flame temperature most similar to that of the reference condition with air. When the recycle rate decreases from OF 25 to OF 27 and OF 29 conditions, the flame temperature increases. This occurs since the amount of recycled flue gas that cools the flame is reduced. In Figure 7b, far from the burner, the temperature distributions become more equal to each other.

The $O_2$ profiles 215 mm from the burner are given in Figure 8a. The error bars show the maximum deviation from the time average during a sampling sequence (8−10 min). In the air and OF 25 flames a large amount of oxygen is present at the centerline of the furnace with concentrations from 5 to 7 vol %. Instead, in the OF 27 and OF 29 cases, the $O_2$ concentrations are close or equal to zero at the centerline. In Figure 8b, for both OF 25 and air-fired conditions, the centerline concentration of CO is below 0.5 vol %, whereas for OF 27 and OF 29 this concentration is much higher. In the two latter cases, the oxygen is consumed rapidly in the proximity of the centerline under strongly reducing conditions. Figure 8c shows the NO concentration. On the centerline, the NO concentration peaks in the air and the OF 25 cases where there are high concentrations of fuel and oxygen as well as high temperatures. In contrast, for OF 27 and 29 the lowest measured NO concentration at the centerline is detected 215 mm from the burner. Moreover, in the OF 27 and 29 flames, the recycled NO that enters the reactor together with the RFG flow is reduced in an environment represented by low oxygen content and high CO concentrations, an environment in which reduction of NO via reburning is likely to occur. As was discussed previously, Okazaki et al.[3] conclude that the main part of the reduction of NO emissions (50−80% in their study) takes place in the combustion zone. Nozaki et al.[18] draw similar conclusions from their experiments in a 1.2 MW test unit: elevated concentrations of HCN and $NH_3$ were observed in the near burner zone during oxy-fuel compared to air conditions, which was assumed to be caused by the reduction of recycled $NO_x$. Reducing zones are found also in the experimental results presented here for the oxy-fuel flames with 27 and 29 vol % oxygen as observed in Figure 8. However, the extension of the reducing zones may vary significantly between different oxy-fuel flames, although the difference in recycle rate is small: the OF 25 flame instead exhibited oxidizing conditions in port 2 and low content of CO.

In Figure 9a the emissions (in mg/MJ) at the outlet are summarized (for the tests with $\lambda = 1.18$). The emission per unit of fuel energy supplied is reduced to about 25% for OF 25 compared to air-fired conditions. There are only small differences in the reduction of NO related to the $O_2$ fraction in the feed gas. Figure 9b shows oxy-fuel tests where the stoichiometric ratio was varied, while keeping the oxygen fraction in the feed gas constant at 27 vol %. The tests were performed both with and without simulated air leakage. The stoichiometry (for $1.18 < \lambda < 1.41$) has little effect on the NO emission (as noted previously, similar results are reported by Kiga et al.[19]). In addition, in the tests with simulated air leakage, an air flow corresponding to about 4% of the total feed-gas flow was introduced as carrier gas. The $CO_2$ concentration decreased during the air leakage tests down to about 55 vol % at steady state, which corresponds to an increased share of $N_2$ in the feed gas from about 1 to 15 vol %. Despite this increase in airborne $N_2$, there was no significant change in the NO emission. Hence, for the present temperature conditions, the formation of thermal and prompt NO was negligible (as expected).

**2. Results from Evaluation of Experimental NO Data.** To evaluate the experiments, the three reaction rates expressed by eq 6 (three rate constants and three activation energies) for reactions 7−9 are determined by a least-squares fit to the experimental data of the air and OF 25 cases. Another set of data, the OF 27 case, is then used to verify the consistency of the model results. The measurement data from the OF 29 case were not used due to the similarity between the OF 27 and OF 29 data; i.e., no additional information would be obtained from comparison with this case. Figure 10 shows the axial profiles of $O_2$, CO, and temperature used as input to the modeling of the one-dimensional combustor. The values are derived from the lateral mean value of the measurements within the MRS.

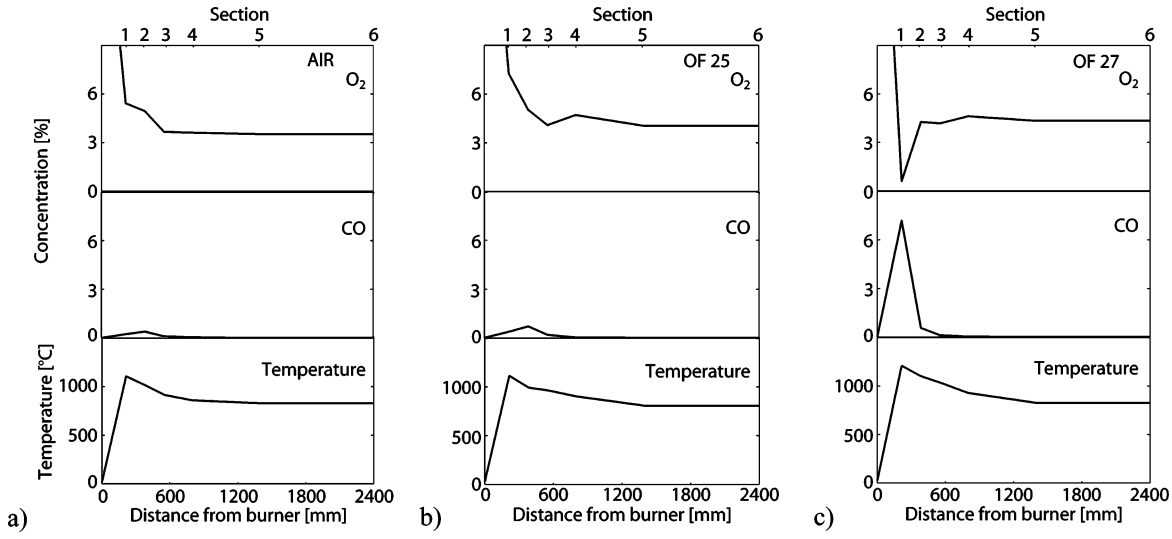


**Figure 10.** Axial temperatures and concentrations of $O_2$ and CO used in the modeling of the air, OF 25, and OF 27 conditions.

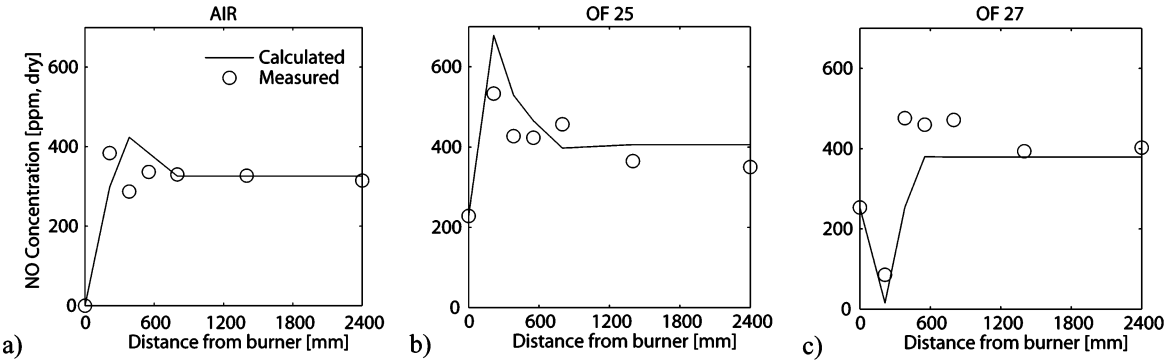


**Figure 11.** Modeled NO fractions compared with the mean values of the experimental data of the given cross sections: (a) air, (b) OF 25, and (c) OF 27.

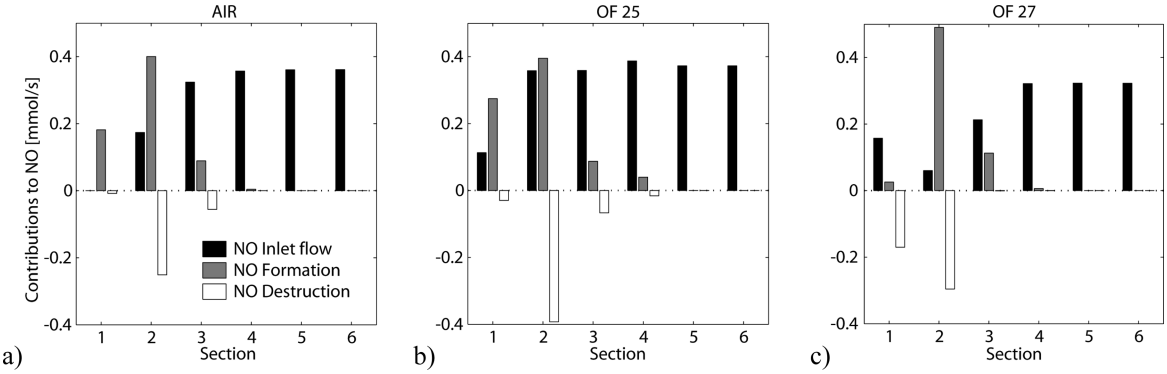


**Figure 12.** Contribution from the sources of NO in each furnace section: (a) air, (b) OF 25, and (c) OF 27.

**Table 7. Total Cumulative Formation and Destruction Rate of NO in Absolute Values and as Percentages of the Air-Fired Case**

| | air | OF 25 | OF 27 |
|---|---|---|---|
| NO formation [mmol/s] | 0.68 (ref) | 0.80 (118%) | 0.64 (94%) |
| NO destruction [mmol/s] | 0.31 (ref) | 0.51 (161%) | 0.47 (148%) |

In Figure 11, modeling and experimental NO data are compared in all three test cases. The largest deviation in the air and OF 25 cases lies in the initial measurement position where the formation of NO for the air-fired case is faster than in the OF 25 case. The OF 27 case is rather well described by the model, using the reaction constants derived from the first set of data. Because of this agreement, it can be said that the model captures the main features of the measurement data in a consistent manner in all three test cases.

The contributions to the NO content in each section from the inlet flow and from formation and destruction of NO are separated from each other by the model. The results are shown in Figure 12. The inlet flow is the quantity of NO that enters each section from the previous one (convection between zones), including recirculated NO. The figure shows important differences in formation and destruction of NO between air combustion and oxy-combustion. The formation of NO from fuel-N increases somewhat from the air case to the OF 25 case, especially in the first section. In the OF 27 case, however, the total formation of NO falls slightly owing to the modest formation in the first section where the oxygen content is almost zero. The activity of the NO reduction mechanism, given by reaction 7, is enhanced during oxy-fuel combustion, with the higher reduction rates of NO being explained by an increased NO content in the reactor, originating from the external recycle flow, and by reducing zones in the combustor with low $O_2$ content. The cumulative rate of NO formation and destruction throughout the reactor are shown in Table 7 for each case. The formation of NO from fuel-N is the same or even slightly higher for oxy-fuel combustion compared to air-firing, while the destruction of NO is about 50% stronger in oxy-combustion. The reduction of NO emission seen in Figure 9a is, thus, explained by an increased activity in the NO gas phase reduction mechanisms, which is investigated in detail in the following section together with optimization possibilities.

**3. Detailed NO Chemistry Modeling Results.** First, the gas phase chemistry in general is analyzed to show the impact of NO reduction. Then the equilibrium relationships for the system $N_2-O_2-NO$ will be illustrated. To quantify the effect of the detailed gas phase chemistry, a reduction ratio of NO ($\psi$) is defined on a molar basis:

$$\psi = 1 - \frac{\mathrm{TFN_{out}}}{\mathrm{NO_{in}}} \tag{10}$$

$NO_{in}$ is the initial molar content of NO in the modeled plug-flow reactor. $TFN_{out}$ (total fixed nitrogen) is the sum of NO + $NO_2$ + HCN + $NH_3$ (i.e., species likely to end up as $NO_x$) calculated at the reactor outlet. The calculations show that in most cases TFN consists exclusively of NO, but $NO_2$ is dominant at low temperatures (<800 °C). Significant quantities of HCN and $NH_3$ are found in areas of high reburning activity.

The Zeldovich mechanism (reactions 2−4) and the reburning mechanism (reactions between hydrocarbons and nitrogen species) were studied separately to determine their individual effects on the $NO_x$ chemistry by isolating in turn each mechanism from the calculation. The results are presented in Figure 13a for calculations at $\lambda = 0.9$. The Zeldovich mechanism is not active at temperatures below 1400 °C, but at higher temperatures the reverse mechanism dominates the NO reduction during oxy-fuel combustion, provided that the concentration of $N_2$ is low. The influence of the reburning mechanism peaks around 900 °C, according to the calculations at $\lambda = 0.9$. This mechanism, however, depends on the combustion conditions in a complex way,[32] and the profile varies in the calculated cases as illustrated in Figure 13b, showing the influence of the

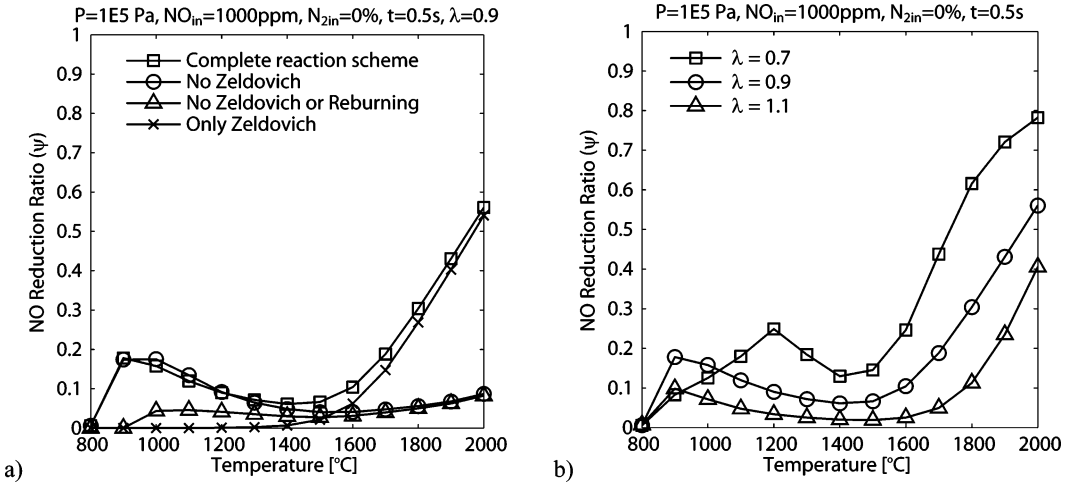


**Figure 13.** NO reduction rate: (a) for isolated reduction mechanisms and (b) for varying stoichiometric ratios.

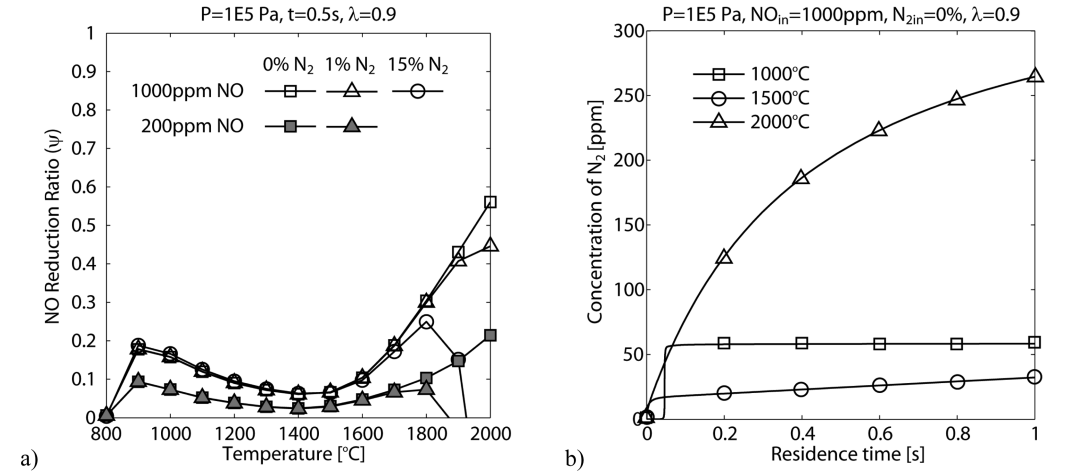


**Figure 14.** (a) Rate of NO reduction at different nitrogen contents in the inlet flow. (b) Formation of $N_2$ from NO as a function of residence time.



stoichiometric ratio on the temperature dependence of reburning. This behavior is similar to what has been observed previously for air-fired combustion.[34] The results also indicate that there is a temperature window between the two reduction mechanisms where the reduction ratio, $\psi$, is low with a minimum at about 1400 °C. As expected, the general trend in Figure 13 is that the reduction of NO is lower at higher stoichiometric ratios when more oxygen is present in the system. In an actual flame, there are zones with a range of stoichiometries, and even though the global stoichiometric ratio is 1.18 for the present experimental conditions, a variety of local stoichiometries will occur. Therefore, reburning is likely to contribute to reduction of NO in all oxy-fuel test cases.

Figure 14a illustrates the effect on the reduction ratio, $\psi$, by the inlet concentrations of $N_2$ and NO to the reactor. At sufficiently high concentration of $N_2$ the thermal mechanism is no longer active in the reverse direction; instead, NO is formed, such as under normal air-fired conditions. The efficiency of the Zeldovich mechanism also decreases at lower initial NO concentration: the critical equilibrium $N_2$ concentration decreases and the reduction of NO becomes slower. The amount of initial NO has an effect on the reburning process[34] as illustrated in Figure 14a, where the reduction ratio at 1000 ppm initial NO is about twice as high as at 200 ppm initial NO content in the reburning region. The elevated NO concentration in the oxidizer of oxy-fuel combustion compared to the concentration during air-firing therefore has a positive effect on both reduction mechanisms investigated.

In Figure 14b, the formation of $N_2$ from reduction of NO is plotted as a function of residence time at $\lambda = 0.9$. The low-temperature mechanism (reburning) is relatively fast and reaches steady state well within 0.1 s. The governing reduction mechanism at high temperatures (Zeldovich) is highly dependent on the residence time and is far from reaching steady state after 1 s even at high temperature. Consequently, the reduction caused by the Zeldovich mechanism shown in Figures 12−14 could be more or less powerful depending on the residence time, while the reburning reduction will stay unaffected by residence time.

With the aim to determine the limits of NO reduction by gas phase mechanisms at a stoichiometric ratio of $\lambda = 1.18$, the equilibrium concentration of NO was calculated in different $N_2$ atmospheres and with the fuel-N content being equal to that in the experiments (Table 1). The results are shown in Figure 15 for an oxidizer containing 70%, 15%, 1%, and 0% $N_2$, typical values for air-firing and for oxy-fuel combustion with different air leakages. The calculated curves represent the equilibrium NO concentrations, which are far lower during oxy-combustion (0−15% $N_2$) than during air-firing (70% $N_2$). Also, the NO concentration if all fuel-N were converted to NO is plotted as a dashed line. Of course, this is a fictitious maximum as some fuel-N certainly will achieve the form of $N_2$. At low temperatures the equilibrium NO concentration is low regardless of the amount of nitrogen in the system, but the calculated concentrations below 1500 °C will never be reached by thermal NO reduction due to the very slow reaction rate of the Zeldovich mechanism at these temperatures (see Figure 14b). Instead, the

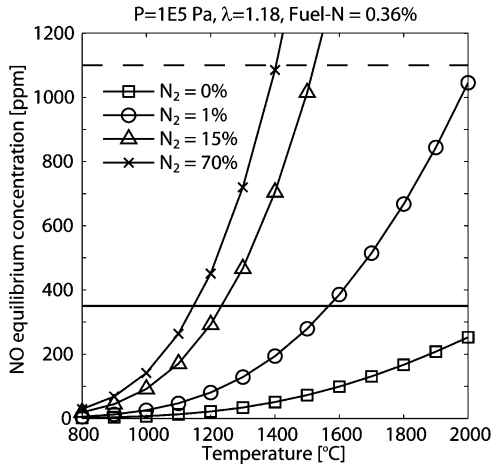


**Figure 15.** Equilibrium concentration of NO. The curves show the equilibrium NO concentration in the gas. The horizontal line is the outlet concentration of NO in the OF 25 case, and the dashed line is the NO concentration if all fuel-N were converted to NO.

NO reduction is due to mechanisms active at low temperature, mainly reburning. The solid line is the NO concentration measured at the outlet of the OF 25 case (maximum $T \approx 1200$ °C), representing the reduction ability at low temperatures. At high temperature the Zeldovich mechanism is active and the $N_2$ concentration in the gas becomes important: if the $N_2$ concentration is high and the equilibrium curve is above the NO concentration from fuel-N (as in an air flame), the well-known thermal NO will be formed. On the other hand, if the $N_2$ concentration is low, as in an oxy-fuel case with pure $O_2$ and little ingress of air into the furnace, the reverse process will take place, and NO will be reduced toward the low equilibrium condition. Opposite to the situation at 1200−1300 °C (Figure 9), there is a great deal to gain by keeping the amount of $N_2$ low at high temperatures, to allow a powerful reduction of NO to take place.

## Conclusions

The focus of this investigation is on NO chemistry in lignite-fired oxy-fuel flames. Gas composition and temperature measurements are presented together with modeling of the combustion chemistry. It is shown that the basic features of NO formation and reduction can be adequately described by a simplistic model coupled to experimental data. In an additional study, special emphasis was put on the gas phase reactions, which were modeled with a detailed chemical kinetic scheme extended to conditions outside the range of the experiments.

During oxy-firing with gas recirculation, the amount of NO emitted per unit of energy supplied is reduced by 70−75% of the emission at air-firing, similar to the conclusions drawn in previous work. In oxy-fuel experiments with simulated air ingress, it is shown that the absence of $N_2$ in oxy-fuel combustion is not important for the overall reduction of NO at the flame temperatures employed in the present work (maximum $T \approx 1300$ °C), i.e., both prompt and thermal NO are of marginal importance, as expected. The modeling of the experimental results shows that the reduction in NO is caused by an increased destruction of formed and recycled NO in oxy-fuel compared to air-fuel conditions. The conversion of fuel-N to NO is similar or even slightly higher during oxy-firing. It should be noted that the results are obtained with a burner that is not specifically designed for low $NO_x$ operation. The influence of oxygen concentration on the NO emission is small in the range of volume fractions of $O_2$ tested (25−29 vol %) at a constant air ratio of 1.18. The amount of excess oxygen also has a modest influence: the NO emission increases by less than 20% when the stoichiometric ratio is raised from 1.18 to 1.41, while keeping the $O_2$ fraction constant at 27 vol %.

The gas phase reaction modeling shows that oxy-fuel combustion has a potential for reduction of NO at high temperature: the absence (or near-zero level) of airborne $N_2$ enables the reverse Zeldovich mechanism to destroy NO at high temperatures. Therefore, in contrast to today's low-$NO_x$ concepts, an optimized oxy-fuel combustor may be designed for operation at high temperatures.

## Acknowledgment

This work was financed by Vattenfall AB. Dr. Valeri Golovitchev is acknowledged for his valuable input to the Chemkin modeling.

## Literature Cited

(1) Glarborg, P.; Jensen, A. D.; Johnsson, J. E. Fuel nitrogen conversion in solid fuel fired systems. *Prog. Energy Combust. Sci.* **2003**, *29*, 89.

(2) Buhre, B. J. P.; Elliott, L. K.; Sheng, C. D.; Gupta, R. P.; Wall, T. F. Oxy-fuel combustion technology for coal-fired power generation. *Prog. Energy Combust. Sci.* **2005**, *31*, 283.

(3) Okazaki, K.; Ando, T. $NO_x$ reduction mechanism in coal combustion with recycled $CO_2$. *Energy* **1997**, *22*, 207.

(4) Hu, Y.; Naito, S.; Kobayashi, N.; Hasatani, M. $CO_2$, $NO_x$ and $SO_2$ emissions from the combustion of coal with high oxygen concentration gases. *Fuel* **2000**, *79*, 1925.

(5) Hu, Y. Q.; Kobayashi, N.; Hasatani, M. The reduction of recycled-$NO_x$ in coal combustion with $O_2$/recycled flue gas under low recycling ratio. *Fuel* **2001**, *80*, 1851.

(6) Hu, Y. Q.; Kobayashi, N.; Hasatani, M. Effects of coal properties on recycled-$NO_x$ reduction in coal combustion with $O_2$/recycled flue gas. *Energy Convers. Manage.* **2003**, *44*, 2331.

(7) Liang, X.; Yan, W.; Li, J.; Yu, Y. Experimental study on $NO_x$ Emission of Pulverized Coal Combustion in $O_2/CO_2$. *Proceedings of the 3rd International Conference on Combustion, Incineration/Pyrolysis and Emission Control*; International Academic Publishers: Beijing, 2004.

(8) Liu, H.; Zailani, R.; Gibbs, B. M. Comparisons of pulverized coal combustion in air and in mixtures of $O_2/CO_2$. *Fuel* **2005**, *84*, 833.

(9) Liu, H.; Zailani, R.; Gibbs, B. M. Pulverized coal combustion in air and in $O_2/CO_2$ mixtures with $NO_x$ recycle. *Fuel* **2005**, *84*, 2109.

(10) Maier, J.; Dhungel, B.; Mönckert, P.; Scheffknecht, G. Coal combustion and emission behaviour under oxy-fuel combustion. *Proceedings of the 31st International technical Conference on Coal Utilization and Fuel Systems*; Coal Technology Association: Gaithersburg, MD, 2006.

(11) Andersson, K.; Mönckert, P.; Maier, J.; Scheffknecht, G.; Johnsson, F. Combustion and flame characteristics of oxy-fuel combustion—Experimental activities within the ENCAP project. *Proceedings of the 8th International Conference on Greenhouse Gas Control Technologies*; IEA Greenhouse Gas R&D Programme: Trondheim, Norway, 2006.

(12) Park, J.; Park, J. S.; Kim, H. P.; Kim, J. S.; Kim, S. C.; Choi, J. G.; Cho, H. C.; Cho, K. W.; Park, H. S. NO emission behavior in oxy-fuel combustion recirculated with carbon dioxide. *Energy Fuels* **2007**, *21*, 121.

(13) Weller, B.; Boiarski, T.; Barrett, R. Experimental evaluation of firing pulverized coal in a $CO_2/O_2$ atmosphere. *Argonne Natl. Lab., [Tech. Rep.] ANL/CNSV-TM* **1985**, *ANL/CNSV-TM-168*.

(14) Kumar, R.; Fuller, T.; Kocourek, R.; Teats, G.; Young, J.; Myles, K.; Wolsky, A. Tests to produce and recover carbon dioxide by burning coal in oxygen and recycled flue gas. *Argonne Natl. Lab., [Tech. Rep.] ANL/CNSV* **1987**, *ANL/CNSV-61*.

(15) Woycenko, D. M.; van de Kamp, W. L.; Roberts, P. A. Combustion of pulverized coal in a mixture of oxygen and recycled flue gas. *IFRF Doc F98/Y/4*; 1995.

(16) Allen, G. Coal combustion in advanced burners for minimal emissions and carbon dioxide reduction technologies. *Report from the Joule II programme, Report No. 26428*; 1995.

(17) Kimura, N.; Omata, K.; Kiga, T.; Takano, S.; Shikisima, S. The characteristics of pulverized coal combustion in $O_2/CO_2$ mixtures for $CO_2$ recovery. *Energy Convers. Manage.* **1995**, *36*, 805.

(18) Nozaki, T.; Takano, S.; Kiga, T. Analysis of the flame formed during oxidation of pulverized coal by an $O_2-CO_2$ mixture. *Energy* **1997**, *22*, 199.

(19) Kiga, T.; Takano, S.; Kimura, N.; Omata, K.; Okawa, M.; Mori, T.; Kato, M. Characteristics of pulverized-coal combustion in the system of oxygen/recycled flue gas combustion. *Energy Convers. Manage.* **1997**, *38*, 129.

(20) Croiset, E.; Thambimuthu, K. V. $NO_x$ and $SO_2$ emissions from $O_2$/$CO_2$ recycle coal combustion. *Fuel* **2001**, *80*, 2117.

(21) Chui, E. H.; Douglas, M. A.; Tan, Y. Modeling of oxy-fuel combustion for a western Canadian sub-bituminous coal. *Fuel* **2003**, *82*, 1201.

(22) Chui, E. H.; Majeski, A. J.; Douglas, M. A.; Tan, Y.; Thamibimuthu, K. V. Numerical investigation of oxy-coal combustion to evaluate burner and combustor design concepts. *Energy* **2004**, *29*, 1285.

(23) Sangras, R.; Farzan, H.; Lu, Y.; Chen, S.; Bose, A. C. Oxy-combustion process in pulverized coal-fired boilers: a promising technology for $CO_2$ capture. *Proceedings of the 31st International technical Conference on Coal Utilization and Fuel Systems*; Coal Technology Association: Gaithersburg, MD, 2006.

(24) Tan, Y.; Croiset, E.; Douglas, M. A.; Thambimuthu, K. V. Combustion characteristics of coal in a mixture of oxygen and recycled flue gas. *Fuel* **2006**, *85*, 507.

(25) Andersson, K.; Johnsson, F. Flame and radiation characteristics of gas-fired $O_2$/$CO_2$ combustion. *Fuel* **2007**, *86*, 656.

(26) *Aspen Plus*, v 2004.1; Aspen Tech.

(27) Abbas, T.; Costa, M.; Costen, P.; Godoy, S.; Lockwood, F. C.; Ou, J. J.; Romo-Millares, C.; Zhou, J. $NO_x$ formation and reduction mechanisms in pulverized coal flames. *Fuel* **1994**, *73*, 1423.

(28) Lutz, A. E.; Kee, R. J.; Miller, J. A. SENKIN: A Fortran Program for Predicting Homogeneous GasPhase Chemical Kinetics with Sensitivity Analysis. *Sandia Natl. Lab. Rep.* **1988**, *87-8248*.

(29) Kee, R. J.; Rupley, F. M.; Miller, J. A. Chemkin-II: A Fortran Chemical Kinetics Package for the Analysis of Gas-Phase Chemical Kinetics. *Sandia Natl. Lab. Rep.* **1990**, *SAND89-8009*.

(30) Glarborg, P.; Alzueta, M. U.; Dam-Johansen, K.; Miller, J. A. Kinetic Modeling of Hydrocarbon/Nitric Oxide Interaction in a Flow Reactor. *Combust. Flame* **1998**, *115*, 1.

(31) Skreiberg, Ø.; Kilpinen, P.; Glarborg, P. Ammonia chemistry below 1400K under fuel-rich conditions in a flow reactor. *Combust. Flame* **2004**, *136*, 501.

(32) Coda Zabetta, E.; Hupa, M.; Saviharju, K. Reducing $NO_x$ Emissions Using Fuel Staging, Air Staging, and Selective Noncatalytic Reduction in Synergy. *Ind. Eng. Chem. Res.* **2005**, *44*, 4552.

(33) Reynolds, W. C. *The Element Potential Method for Chemical Equilibrium Analysis: Implementation in the Interactive Program STANJAN*; Department of Mechanical Engineering, Stanford University, 1986.

(34) Alzueta, M. U.; Bilbao, R.; Millera, A.; Glarborg, P.; Østberg, M.; Dam-Johansen, K. Modeling Low-Temperature Gas Reburning. $NO_x$ Reduction Potential and Effect of Mixing. *Energy Fuels* **1998**, *12*, 329.

*Received for review* August 31, 2007
*Revised manuscript received* November 13, 2007
*Accepted* November 29, 2007

IE0711832